

Nanoscale

Accepted Manuscript



This is an *Accepted Manuscript*, which has been through the Royal Society of Chemistry peer review process and has been accepted for publication.

Accepted Manuscripts are published online shortly after acceptance, before technical editing, formatting and proof reading. Using this free service, authors can make their results available to the community, in citable form, before we publish the edited article. We will replace this *Accepted Manuscript* with the edited and formatted *Advance Article* as soon as it is available.

You can find more information about *Accepted Manuscripts* in the [Information for Authors](#).

Please note that technical editing may introduce minor changes to the text and/or graphics, which may alter content. The journal's standard [Terms & Conditions](#) and the [Ethical guidelines](#) still apply. In no event shall the Royal Society of Chemistry be held responsible for any errors or omissions in this *Accepted Manuscript* or any consequences arising from the use of any information it contains.

ARTICLE

Synthesis of 3D Structured Graphene as High Performance Catalyst Support for Methanol Electrooxidation

Cite this: DOI: 10.1039/x0xx00000x

Yecheng Li,^a Lei Zhang,^b Zhuofeng Hu,^b and Jimmy C. Yu^{*a,b}Received 00th January 2012,
Accepted 00th January 2012

DOI: 10.1039/x0xx00000x

www.rsc.org/

A simple process for preparing 3D structured graphene (3D-G) by a solution combustion method is reported. The product was deposited with platinum and used for methanol electrooxidation. The catalyst shows considerable enhancement on both activity and stability towards methanol electrooxidation reaction. Characterizations reveal that the Pt/3D-G catalyst has a more negative onset potential as well as a higher electrochemically active specific surface area compared with a commercial Pt/C catalyst. Moreover, the catalyst exhibits higher tolerance to corrosion than carbon black. This work provides an efficient way for preparing 3D-G as a promising support for the oxidation of small organic molecules in fuel cells.

Introduction

Direct-methanol fuel cells (DMFCs) have been regarded as an emerging green technology owing to low cost, industrial-scale availability, and high energy density of liquid methanol.¹⁻³ Although a lot of efforts have been made, there are still two major challenges precluding large-scale commercial applications: insufficient reliability and high cost.⁴ While platinum possesses reasonable activity for electrocatalytic methanol oxidation, the exploration of advanced catalyst support is a promising route to obtain durable electrocatalysts of even higher efficiency.⁵ Several studies used large surface area catalyst supports such as carbon black, carbon nanofibers, carbon nanotubes, porous silicon structures and graphene,⁶⁻⁹ taking advantage of their excellent conductivity, loading ability and facileness. In particular, three-dimensional (3D) Pt-decorated porous materials often exhibit improved electrocatalytic properties due to the wide spread of Pt nanoparticles in the architectures.^{10, 11}

Graphene, especially 3D structured graphene (or graphene foam) is an ideal candidate for noble metal catalysts support in DMFCs because of its high electron conductivity, large surface area, sufficient porosity and thermal stability.¹² Many strategies have been exploited for the fabrication of 3D graphene. For example, Chen and his co-workers¹³ used CVD method to

obtain graphene foam with large holes in size of a few hundred micrometers, with nickel foam as a sacrificial template. 3D structured graphene can also be obtained from graphene oxide. Functionalized silica or polystyrene sphere was used to assemble graphene oxide into a 3D mixture by electrostatic force. After etching away the template, a porous structured graphene material could form.¹⁴ Reduction of graphene oxide via different reducing agents such as L-ascorbic acid, NaHSO₃, Na₂S and HI,^{15, 16} or by electrochemical reduction method¹⁷ can also result in the formation of 3D structured graphene. However, mass production of 3D structured graphene at a low cost remains a challenge.

The solution combustion method is a proven technology for the preparation of nanocrystalline metal oxides.^{18, 19} This method, involving redox reactions between oxidizer and fuel, is simple, instantaneous, cost-effective, and environmentally benign. During the process, evolution of large volumes of gases (CO₂, N₂ and H₂O) results in a highly voluminous product. For the synthesis of metal oxide, a high temperature such as 800 °C was usually adopted. However, for preparation of carbon materials, one cannot utilize solution combustion method at such high temperature. Herein, we exploited a low temperature solution combustion method to fabricate a 3D structured graphene with porous structure from graphene oxide. The

product thus obtained can be used as a Pt catalyst support for methanol electrooxidation. This Pt/3D-G electrocatalyst displays both higher electrocatalytic activity and higher durability than the conventional Pt/C catalyst in DMFCs.

Experimental details

Chemicals: All chemicals used can be purchased commercially and have the highest possible purities. Commercial state-of-the-art 20 wt% Pt/C (Johnson Matthey Company, HiSPEC™ 3000) was used as the benchmark for comparison and was denoted as Pt/C.

Synthesis: Graphene oxide (GO) was prepared by a modified Hummer method.²⁰ In a typical synthesis, 2g of graphite were added into a 80 °C solution of concentrated sulfuric acid (12 mL), P₂O₅ (2.5 g) and K₂S₂O₈ (2.5 g). The reaction was allowed to proceed for 24 h under vigorous stirring. To this mixture, 500mL of deionized (DI) water was added slowly. The solution was then filtered and washed with DI water until the rinse water became pH neutral. The filter cake was dried at room temperature to obtain the preoxidized graphite. Then it was added into 120 mL of concentrated sulfuric acid and 30 mL of concentrated nitric acid in an ice bath. Next, 15 g KMnO₄ was slowly added into the above solution under stirring. Once mixed, the solution was raised to 35 °C in an oil bath and stirred for about 96 h, forming a thick paste. Afterwards, 1 L distilled water was added to obtain an olive solution. This was followed by the addition of 1 L distilled water and slow addition of 20mL of H₂O₂ (30%), turning the color of the solution from dark brown to yellow. Finally, the solution was cooled to room temperature, and then filtered with 1 L HCl (1:10) and DI water until the rinse water became neutral. The yellow cake-like product was dried in vacuum at room temperature for further use. For the fabrication of 3D structured graphene, 2 mL aqueous suspensions of GO at concentrations of 6 mg/mL were prepared, and 0.2 g glycine as fuel was added into the solution. After being ultrasonicated for 30 min, the combined solution was heated to 150 °C, resulting in a thick colloidal suspension. This colloidal solution was then heated to 250°C for 30 seconds in air. The thermal treatment resulted in evolution of vapors, leaving a black voluminous product. The product was washed several times with DI water, followed by washing with ethanol and dried at 60 °C. The final product was denoted as 3D-G. Pt nanoparticles supported on 3D-G were prepared by a solution reduction process with NaBH₄ as a reducing agent. The total Pt loading on the support was 20 wt%. An appropriate amount of H₂PtCl₆ and 50 mg of 3D-G were suspended in 2mL of acetone. After vacuum dried, 0.5 M NaBH₄ (0.5 mL) was added to the mixture. After the reduction, the mixture was washed with water followed by ethanol and dried in air at 60°C.

Characterization: Morphology of the products was characterized by scanning electron microscopy (SEM) on a FEI Quanta 400 microscope and by transmission electron microscopy (TEM) on a CM-120 microscope (Philips, 120 kV).

X-Ray Diffraction (XRD) patterns were recorded with a Rigaku SmartLab X-ray diffractometer using Cu K α irradiation ($\lambda=1.5406\text{\AA}$). The accelerating voltage and applied current were 40 kV and 40 mA. X-Ray photoelectron spectroscopy (XPS) was performed using a Sengyang SKL-12 spectrometer equipped with a VG CLAM 4 MCD electron energy analyzer and twin anode Mg K α radiation (1253.6 eV) or Al K α radiation (1496.3 eV) X-ray sources. The FTIR spectra of different samples were recorded from KBr pellets (Aldrich, 99%, FT-IR grade) with a Nicolet 560 Ft-IR spectrophotometer. Inductively coupled plasma optical emission spectroscopy (ICP-OES) characterizations were performed on a PerkinElmer Optima 4300DV system. Raman spectra were collected on a RM-1000 Micro Raman Spectrometer.

Electrochemical measurements: Electrochemical experiments were conducted with a CHI 660C electrochemical workstation, using a standard three electrode cell, with a Pt foil ($1.0 \times 1.0 \text{ cm}^2$) serving as the counter electrode, a Ag/AgCl electrode in saturated potassium chloride serving as the reference electrode and a glassy carbon (GC) disk (5 mm in diameter) with coated catalysts serving as the working electrode. The working electrode was fabricated as follows: 20 mg of catalyst powder was dispersed in 1 mL of 0.05% Nafion solution in ethanol with ultrasonication for 30 min to form a homogeneous black suspension. Then 8 μL of the resulting suspension was carefully dropped onto the GC electrode surface, and the coating was dried at room temperature for 10 minutes. For preadsorbed CO (CO_{ad}) stripping measurements, pure CO was first bubbled into 0.5 M H₂SO₄ solution for 15 min to allow the complete adsorption of CO onto the catalyst while the working electrode was still at 0 mV vs saturated Ag/AgCl electrode. Then excess CO in the electrolyte was purged out with N₂ for 10 min. The CO stripping voltammograms were measured by oxidation of the CO_{ad} in the 0.5 M H₂SO₄ and the amount of CO_{ad} was measured by integration of the CO_{ad} stripping peak. The electrocatalytic activity of the catalysts for the methanol oxidation was examined by collecting CVs in a N₂-purged 0.5 M H₂SO₄ and 1 M methanol solution at a scan rate of 50 mV/s. Several activation scans were performed until the stable voltammogram curves were obtained. Only the last voltammograms were used for comparing the catalytic activity of the specified catalysts. The chronoamperometry tests were performed at 0.65 V for a period of 6000 s at room temperature. The chronopotentiometric curves were recorded in a 0.5 M H₂SO₄ and 1 M methanol solution.

Results and Discussion

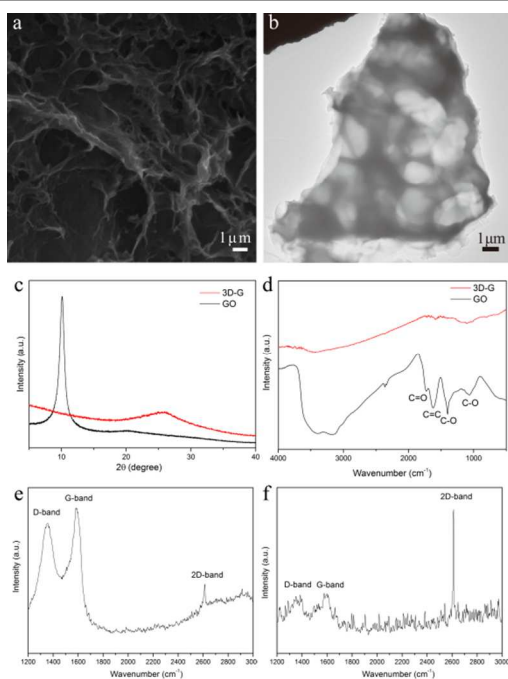


Figure 1. (a) SEM image and (b) TEM image for the as prepared 3D-G. (c) XRD patterns for 3D-G and GO. (d) FTIR spectra for 3D-G and GO. (e, f) Raman spectra for 3D-G.

The 3D structured graphene was synthesized by a solution combustion method. Before heating, GO was well dispersed in water to form a stable aqueous suspension of 6 mg/mL under ultrasonication. Glycine was then added to the solution as a fuel for further combustion. The solution was heated to 150 °C on a hotplate and after water vaporized, a thick colloidal suspension was formed at the bottom. The suspension was immediately transferred to an oven at 250 °C. The glycine would be ignited under this condition and generated a lot of gas in the graphene oxide suspension. After 30 seconds, the combustion finished and the suspension turned to black powder with much increased volume. This synthetic route can be easily expanded to gram scale with a larger container. Fig.1a and Fig.1b show the scanning electron microscope (SEM) and transmission electron microscope (TEM) images of the as-prepared graphene material. After the combustion, the GO sheets turned into an interconnected porous network, similar to reported 3D graphene structures.^{15, 21} In 250 °C circumstance, the glycine ignited and reacted with oxidizers such as oxygen or carboxyl, hydroxyl groups on the graphene oxide surface. A lot of bubbles composed of N₂, CO₂ and H₂O were generated in the GO suspension and between graphene oxide sheets. As a result, pores were formed by the bubbles between layers of graphene sheets. Because the bubbles generated by combustion had random sizes, the resulting pores in the architecture had uneven sizes. The product, denoted as 3D-G, showed a foam-like structure with many pores and expanded volume compared to the GO suspension. Fig.1c shows the XRD patterns of graphene oxide and the as-prepared 3D structured graphene. A typical broad peak near 10° was observed for the GO powder.²² After

the combustion treatment, the disappearing peak indicated the efficient exfoliation of the multilayer GO and a new broad diffraction peak at 25° suggested the transformation to graphene 2D sheets with removal of surface functional groups.²³ The FTIR spectra of GO showed characteristic -OH (~3450 cm⁻¹), C=C (~1620 cm⁻¹), and carbonyl (~1730 cm⁻¹, 1400 cm⁻¹ and 1060 cm⁻¹) peaks, which confirmed the existence of carboxyl and hydroxyl groups on the graphene oxide surface. After the combustion, nearly all peaks were eliminated except for the band at 1620 cm⁻¹, which could be attributed to aromatic carbon double bonds.²⁴ The FTIR further proves that during the combustion method, the functional groups in the GO were removed and graphene sheets were formed. Fig.1e and Fig.1f show the Raman spectra of 3D-G in different areas of a same sample. The intensity ratio of the 2D band to G band was very different in these two spectra. It has been reported that the I_{2D}/I_G could be used to determine the layer number of graphene.²⁵ In Fig. 1f, the I_{2D}/I_G is 2.4, referring to single layered graphene. On the other hand, an I_{2D}/I_G value less than 1 shown in Fig. 1e represents a multilayer graphene structure. The Raman spectra show the structure complexity in the interconnected porous network of graphene.

Conventionally, chemically reduced graphene oxide (rGO) was produced from graphene oxide with different reductants such as hydrazine,²⁶ hydroquinone,²⁷ sodium borohydride,^{28, 29} and ascorbic acid.³⁰ Usually a thermal treatment was also needed and the reaction time varied from 2 hours to 24 hours. Few layered graphene sheets were common products with residual oxygen groups which can be seen from FTIR. It is very difficult to obtain good quality single layered rGO sheets which can be identified from the Raman spectra or AFM. However, the FTIR and Raman spectra of the as-prepared 3D-G show that the simple combustion method can achieve graphene sheets with good quality. No costly reagents were needed in the process and the reaction is almost instantaneous.

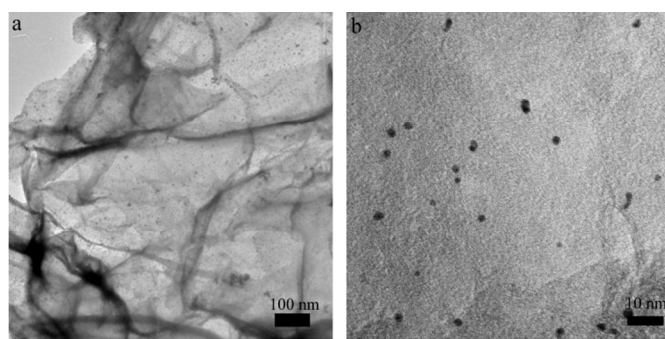


Figure 2. (a) Low magnification TEM image of Pt/3D-G. (b) High magnification TEM image of Pt/3D-G.

The 3D structured 3D-G could be an ideal candidate as a catalyst support. We prepared Pt deposited 3D-G with a solution reduction method. The as-prepared 3D-G was suspended in an acetone solution of H₂PtCl₆. The mixture was homogenized by ultrasonication and then vacuum dried. NaBH₄ solution was then added to reduce the platinum. By this method, homogenous deposited Pt nanoparticles on the 3D-G

could be achieved. From the low magnificant TEM images in Fig.2a, it can be seen that the Pt nanoparticles are anchored on the transparent 3D-G homogeneously on the framework. The high magnificant TEM images in Fig.2b disclosed homogenous Pt nanoparticles in size of 3 nm. The distribution of Pt was very good and few aggregating particles were observed. The actual content of Pt was measured by inductively coupled plasma (ICP) to be 18.9 wt%, close to the theoretical value of 20.0 wt%.

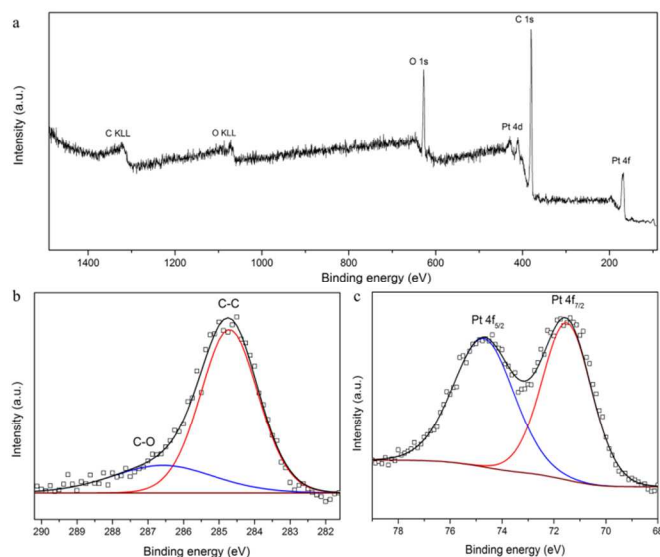


Figure 3. XPS spectra of Pt/3D-G.

To further evaluate the chemical composition of the Pt/3D-G architecture, X-ray photoelectron spectroscopy (XPS) measurements were carried out. The survey scan in Fig 3a showed only peaks of C, O and Pt. As shown in Fig. 3b, the peak fitting indicates the presence of a well-defined peak for C 1s at a binding energy of 284.7 eV. Meanwhile, a small peak at 286.8 eV was also observed indicating the presence of C-O bonding which belongs to the residual carboxyl groups on the graphene surface. The C1s XPS spectrum of the catalyst showed minimal carbon-oxygen peaks proving the good quality of 3D-G.³¹ Fig. 3c shows the Pt 4f XPS spectra. Metallic Pt at the two binding energies of 71.5 and 74.7 eV demonstrate the successful deposition of platinum on the 3D-G.³² There was only Pt (0) species existed on the surface of catalyst. The crystalline structure of the Pt/3D-G catalyst was investigated by XRD as shown in Fig.4. It exhibited typical diffraction peaks of platinum with face-centred cubic structure for Pt (111), Pt (200).

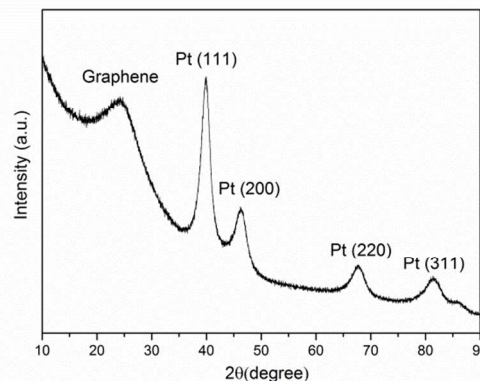


Figure 4. XRD pattern of Pt/3D-G.

Next we tested the catalyst in electrocatalytic reaction and compared it with commercial Pt/C bought from the Johnson Matthey Company. The cyclic voltammograms (CVs) were recorded with samples in an electrolyte containing 0.5 M H₂SO₄ and 1M MeOH. The activities of catalysts were normalized by the mass of Pt. Fig.5a shows that the peak current density for methanol oxidation on Pt/3D-G is 443 mA·mg⁻¹ Pt, which is about 50% higher than the peak current density on Pt/C (295 mA·mg⁻¹ Pt). The onset potential of Pt/3D-G toward methanol (0.17 V) is more negative than that of Pt/C (0.26V), indicating a greater catalytic activity for methanol electrooxidation. There are reports using nitrogen doped carbon/graphene composites³³ or mixture of graphene and carbon nitride³⁴ as support for Pt toward methanol oxidation. Their highest activity is 603 mA·mg⁻¹ Pt and 15.7 mA·cm⁻². Here we show that the 3D structured graphene is also a good support for platinum and the composite catalyst exhibits an activity as high as 443 mA·mg⁻¹ Pt and 17 mA·cm⁻².

Moreover, the ratio of the forward anodic peak current density (I_f) to the reverse anodic peak current density (I_b) can be used to evaluate the catalyst tolerance to the intermediate carbonaceous species accumulated on electrode surface.³⁵ The I_f/I_b ratios are estimated as 0.87 and 0.66 for Pt/3D-G and Pt/C, respectively. The carbon black, which is used as catalyst support in the commercial Pt/C, is known to corrode under high potentials in DMFCs. The low I_f/I_b ratio of Pt/C also proved a bad tolerance to poisoning. A higher I_f/I_b ratio of Pt/3D-G indicated the higher efficiency of oxidation of methanol during the forward anodic scan with less accumulation of carbonaceous residues. For further comparison, another sample with 9 wt% Pt loading on 3D-G was prepared and compared with commercial Pt/C in Fig 5b. The activities were normalized to the electrode area. Although this sample has only nearly half the Pt content compared to the commercial 20 wt% Pt/C, they have nearly the same peak current. And the I_f/I_b is even higher at 1.34, which implies a much better tolerance to intermediate carbonaceous poisoning.

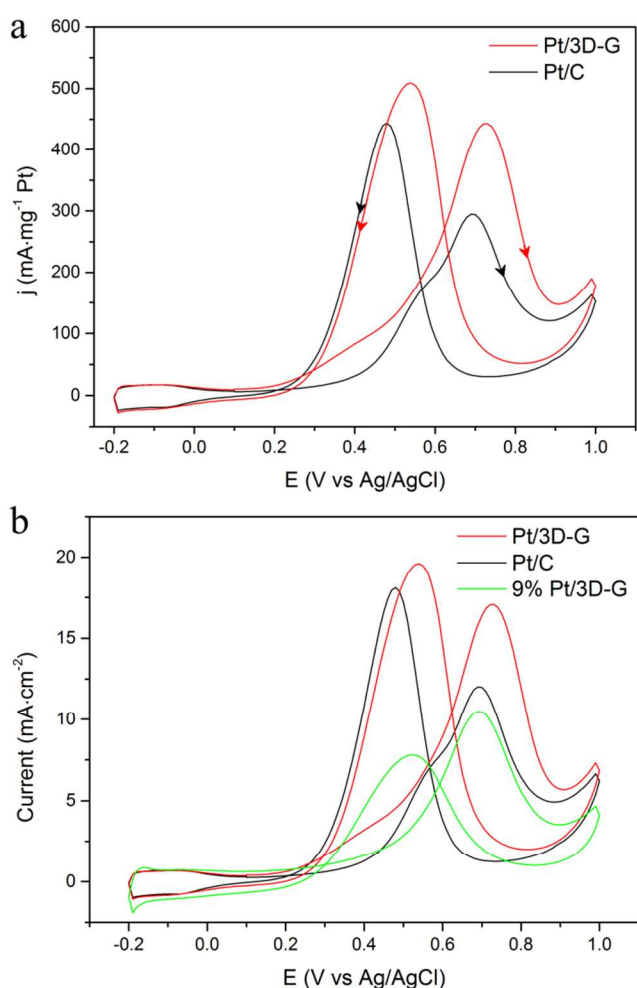


Figure 5. Electrochemical activities of the catalysts normalized to mass (a) and area (b) recorded at 50 mV/s in 0.5M H₂SO₄ and 1M methanol solution.

The CO stripping method was used to evaluate the electrochemically active specific surface area (ECSA) of the catalysts. The electrode was first purged with pure CO to achieve saturated adsorbed CO on the catalyst. Then the adsorbed CO was electro-oxidized on the catalyst and the charge was used to calculate the actual active surface area. The CO stripping voltammograms for Pt/3D-G and Pt/C was shown in Fig.6. A second CV scan after the electrooxidation was used as the background current. The onset potential toward CO_{ad} oxidation on Pt/3D-G (0.25V) was more negative than that observed for CO_{ad} oxidation on Pt/C (0.35V). This indicated that Pt/3D-G has a greater ECSA than Pt/C. The lower onset potential showed that CO could be more easily removed from the catalyst in Pt/3D-G which would relief the catalyst from poisoning. The actual active surface area was calculated from the CO_{ad} oxidation charge after subtracting the background current using the following equation:

$$S_{CO} = \frac{Q_{CO}}{0.42 \text{ mC} \cdot \text{cm}^{-2}}$$

where Q_{CO} is CO_{ad} oxidation charge and $0.42 \text{ mC} \cdot \text{cm}^{-2}$ corresponds to the charge needed for the oxidation of a monolayer of adsorbed CO on the surface.^{36, 37} The ECSA of Pt/3D-G was calculated to be $121 \text{ m}^2/\text{g}$, which was larger than that of Pt/C ($86 \text{ m}^2/\text{g}$). Another interesting phenomenon that should be noted from the voltammograms is that the 3D-G showed a much larger double layer capacitance compared to carbon black in the Pt/C catalyst. This implies a possible application of this material in energy storage field.

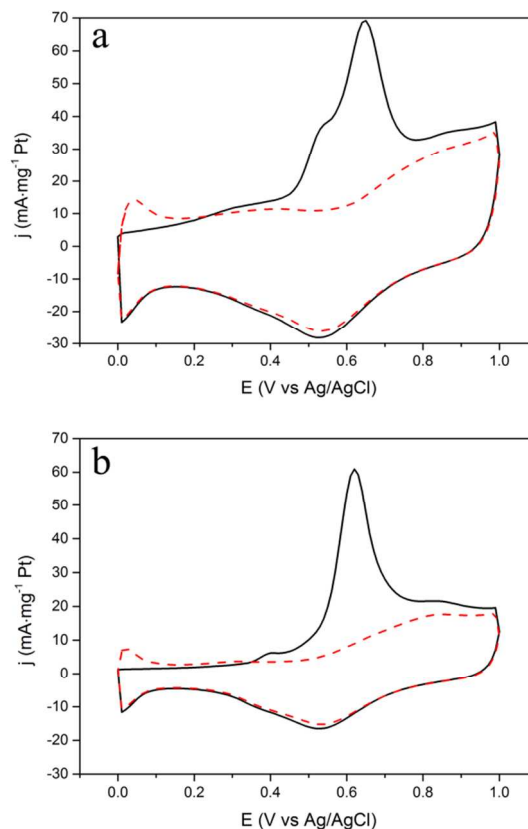


Figure 6. CO stripping voltammograms for (a) Pt/3D-G and (b) Pt/C.

The long-term stability is one of the critical factors for a practical catalyst. To evaluate the stability of the catalysts, the chronoamperometric measurements were conducted at a potential value of 0.65 V vs. Ag/AgCl (Fig.7). The Pt/3D-G catalyst showed both a slower deterioration rate and a higher steady-state current than the Pt/C catalyst. After 6000 seconds, the commercial Pt/C catalyst lost 84.2% current density probably due to the corrosion of the catalyst and formation of adsorbed CO, which poisons the catalytically active sites. However, the new Pt/3D-G lost only 74.9% efficiency which is obviously lower than commercial one. This demonstrates that Pt/3D-G has higher tolerance to poisoning in the electrolyte solution than the commercial Pt/C. The electrochemical properties of the catalysts are summarized in Table 1.

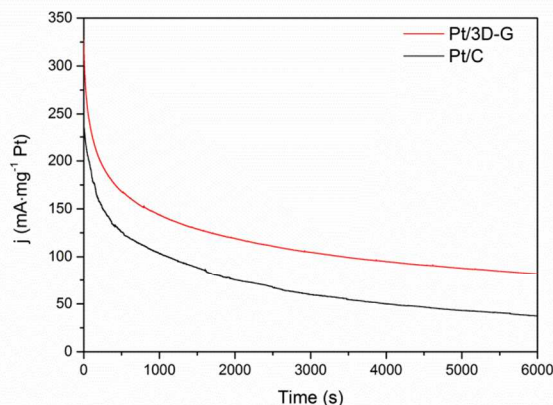


Figure 7. Chronoamperometric responses recorded at 0.65 V (vs. Ag/AgCl) for Pt/3D-G and commercial Pt/C.

Table 1. Summary comparing Pt/3D-G and Pt/C catalysts for methanol electrooxidation

Catalyst	Pt/3D-G	Pt/C
Onset potential toward CO _{ad} oxidation	0.25 V	0.35 V
Electrochemically active specific surface area (ECSA)	121 m ² /g	86 m ² /g
Onset potential toward methanol oxidation	0.17 V	0.26 V
Peak current density of methanol oxidation	443 mA·mg ⁻¹ Pt	295 mA·mg ⁻¹ Pt
Specific activity	3.7 A/m ²	3.4 A/m ²

Conclusions

In summary, we present a scalable template-free energy-efficient approach to synthesize a novel hierarchical porous graphene framework material. Owing to the unique textural features, a 3D structured graphene supported Pt catalyst shows a greater catalytic surface area, greater electrocatalytic activity and slower deterioration rate and greater steady-state current than a conventional Pt/C catalyst toward methanol electrooxidation. We believe that the 3D-G has promising applications as catalyst support in fuel cells and can be extended to other applications in catalysis, sensor and energy storage.

Acknowledgements

This work was partially supported by the Research Grants Council of the Hong Kong Special Administrative Region, China, under Theme-based Research Scheme through Project No. T23-407/13-N and a grant from the Shenzhen Basic Research Scheme (JCYJ20120619151417947).

Notes and references

^a Environmental Science Programme, School of Life Sciences, The Chinese University of Hong Kong, Shatin, N.T., Hong Kong SAR, P. R. China.

^b Department of Chemistry, The Chinese University of Hong Kong, Shatin, N.T., Hong Kong SAR, P. R. China. E-mail: jimyu@cuhk.edu.hk.

- C. K. Brozek and M. Dincă, *Journal of the American Chemical Society*, 2013, **135**, 12886-12891.
- D. Sun, Y. Fu, W. Liu, L. Ye, D. Wang, L. Yang, X. Fu and Z. Li, *Chemistry – A European Journal*, 2013, **19**, 14279-14285.
- J. Liu, G.-H. Kim, Y. Xue, J. Y. Kim, J.-B. Baek, M. Durstock and L. Dai, *Advanced Materials*, 2014, **26**, 786-790.
- R. Borup, J. Meyers, B. Pivovar, Y. S. Kim, R. Mukundan, N. Garland, D. Myers, M. Wilson, F. Garzon, D. Wood, P. Zelenay, K. More, K. Stroh, T. Zawodzinski, J. Boncella, J. E. McGrath, M. Inaba, K. Miyatake, M. Hori, K. Ota, Z. Ogumi, S. Miyata, A. Nishikata, Z. Siroma, Y. Uchimoto, K. Yasuda, K.-i. Kimijima and N. Iwashita, *Chemical Reviews*, 2007, **107**, 3904-3951.
- E. Antolini, *Applied Catalysis B: Environmental*, 2009, **88**, 1-24.
- S. Han, Y. Wei and B. A. Grzybowski, *Chemistry – A European Journal*, 2013, **19**, 11194-11198.
- Q. Yan, Y. Lin, C. Kong and L. Chen, *Chemical Communications*, 2013, **49**, 6873-6875.
- Y. Zhang, X. Bo, C. Luhana, H. Wang, M. Li and L. Guo, *Chemical Communications*, 2013, **49**, 6885-6887.
- A. S. Arico, P. Bruce, B. Scrosati, J.-M. Tarascon and W. van Schalkwijk, *Nature Materials*, 2005, **4**, 366-377.
- T. Maiyalagan, T. O. Alaje and K. Scott, *The Journal of Physical Chemistry C*, 2011, **116**, 2630-2638.
- C. Hu, H. Cheng, Y. Zhao, Y. Hu, Y. Liu, L. Dai and L. Qu, *Advanced Materials*, 2012, **24**, 5493-5498.
- M. J. Allen, V. C. Tung and R. B. Kaner, *Chemical Reviews*, 2009, **110**, 132-145.
- Z. Chen, W. Ren, L. Gao, B. Liu, S. Pei and H.-M. Cheng, *Nature Materials*, 2011, **10**, 424-428.
- J. L. Vickery, A. J. Patil and S. Mann, *Advanced Materials*, 2009, **21**, 2180-2184.
- W. Chen and L. Yan, *Nanoscale*, 2011, **3**, 3132-3137.
- W. Chen, S. Li, C. Chen and L. Yan, *Advanced Materials*, 2011, **23**, 5679-5683.
- K. Sheng, Y. Sun, C. Li, W. Yuan and G. Shi, *Scientific Reports*, 2012, **2**, 247.
- A. S. Prakash, P. Manikandan, K. Ramesha, M. Sathiya, J. M. Tarascon and A. K. Shukla, *Chemistry of Materials*, 2010, **22**, 2857-2863.
- K. Nagaveni, M. S. Hegde and G. Madras, *The Journal of Physical Chemistry B*, 2004, **108**, 20204-20212.
- W. S. Hummers and R. E. Offeman, *Journal of the American Chemical Society*, 1958, **80**, 1339-1339.
- Y. Xu, K. Sheng, C. Li and G. Shi, *ACS Nano*, 2010, **4**, 4324-4330.
- H. Feng, R. Cheng, X. Zhao, X. Duan and J. Li, *Nature Communications*, 2013, **4**, 1539.

23. Y. Tang, F. Huang, W. Zhao, Z. Liu and D. Wan, *Journal of Materials Chemistry*, 2012, **22**, 11257-11260.
24. G. Goncalves, P. A. A. P. Marques, C. M. Granadeiro, H. I. S. Nogueira, M. K. Singh and J. Grácio, *Chemistry of Materials*, 2009, **21**, 4796-4802.
25. R. John, A. Ashokreddy, C. Vijayan and T. Pradeep, *Nanotechnology*, 2011, **22**, 165701-165707.
26. S. Stankovich, D. A. Dikin, R. D. Piner, K. A. Kohlhaas, A. Kleinhammes, Y. Jia, Y. Wu, S. T. Nguyen and R. S. Ruoff, *Carbon*, 2007, **45**, 1558-1565.
27. G. Wang, J. Yang, J. Park, X. Gou, B. Wang, H. Liu and J. Yao, *The Journal of Physical Chemistry C*, 2008, **112**, 8192-8195.
28. Y. Si and E. T. Samulski, *Nano Letters*, 2008, **8**, 1679-1682.
29. H.-J. Shin, K. K. Kim, A. Benayad, S.-M. Yoon, H. K. Park, I.-S. Jung, M. H. Jin, H.-K. Jeong, J. M. Kim, J.-Y. Choi and Y. H. Lee, *Advanced Functional Materials*, 2009, **19**, 1987-1992.
30. V. Dua, S. P. Surwade, S. Ammu, S. R. Agnihotra, S. Jain, K. E. Roberts, S. Park, R. S. Ruoff and S. K. Manohar, *Angewandte Chemie International Edition*, 2010, **49**, 2154-2157.
31. S. Some, Y. Kim, Y. Yoon, H. Yoo, S. Lee, Y. Park and H. Lee, *Sci. Rep.*, 2013, **3**.
32. K. C. Park, I. Y. Jang, W. Wongwiriyan, S. Morimoto, Y. J. Kim, Y. C. Jung, T. Toya and M. Endo, *Journal of Materials Chemistry*, 2010, **20**, 5345-5354.
33. J. Zhu, M. Xiao, X. Zhao, K. Li, C. Liu and W. Xing, *Chemical Communications*, 2014, **50**, 12201-12203.
34. H. Huang, S. Yang, R. Vajtai, X. Wang and P. M. Ajayan, *Advanced Materials*, 2014, **26**, 5160-5165.
35. W. Liu, A.-K. Herrmann, D. Geiger, L. Borchardt, F. Simon, S. Kaskel, N. Gaponik and A. Eychmüller, *Angewandte Chemie International Edition*, 2012, **51**, 5743-5747.
36. P. Ochal, J. L. Gomez de la Fuente, M. Tsyppkin, F. Seland, S. Sunde, N. Muthuswamy, M. Rønning, D. Chen, S. Garcia, S. Alayoglu and B. Eichhorn, *Journal of Electroanalytical Chemistry*, 2011, **655**, 140-146.
37. T. Vidaković, M. Christov and K. Sundmacher, *Electrochimica Acta*, 2007, **52**, 5606-5613.